CFD SIMULATION OF FORCED CONVECTIVE BOILING IN HEATED CHANNELS

Boštjan Končar
Jožef Stefan Institute, Slovenia
Bostjan.Koncar@ijs.si

Eckhard Krepper
Forschungszentrum Rossendorf, Germany
E.Krepper@fz-rossendorf.de

ABSTRACT

In this paper a forced convective boiling of Refrigerant R-113 in a vertical annular channel has been simulated by a custom version of the CFX-5 code. The employed subcooled boiling model uses a special treatment of the wall boiling boundary, which assures the grid invariant solution. The simulation results have been validated against the published experimental data [1]. In general a good agreement with the experimental data has been achieved, which shows that the current model may be applied for the Refrigerant R-113 without significantly changing the model parameters. The influence of non-drag forces, bubble diameter size and interfacial drag model on the numerical results has been investigated as well.

Introduction

Boiling and the associated heat transfer are some of the most important phenomena which not only affect the reactivity of the nuclear reactors but also determine the criticality of equipment in power generation facilities. Forced convective boiling can occur in narrow flow passages between the heated fuel rods of a pressurized water reactor (PWR) core during startup, nominal or accidental conditions. During accident conditions the critical heat flux (CHF) can be exceeded and my lead to the burnout of the fuel cladding. Therefore it is desirable to be able to understand and predict the convective boiling flows.

The phenomena associated with convective boiling flow and CHF are usually three-dimensional (3D) and very complex, many small-scale processes are not well understood yet. Therefore both, good local experimental data and reliable 3D multi-fluid codes are needed to better understand the boiling flow processes. An experiment with the real steam-water flow to validate numerical predictions would be extremely expensive. Therefore, often Refrigerants were used as a working fluid to simulate forced convective boiling in PWRs at much lower pressures and heat fluxes. Of course the relevant similarity criteria such as density ratio or Boiling number must be used to scale the experiment to the real PWR system [2].

In this paper the Arizona State University (ASU) boiling flow experiments [1] in annular channel were used to validate the simulation capability of the custom CFD code CFX-5. The Refrigerant R-113 at 2.69 bar was used as a working fluid. The subcooled boiling model implemented in the test version of the CFX-5 code [3] is applied and validated in this work. The main improvements considering the wall boiling boundary conditions are also briefly described. The same model has been previously successfully validated [4] against the water-steam experiments in vertical pipes at high

pressure conditions (30 – 150 bar). Further, a sensitivity analysis of non-drag forces, bubble size and interfacial drag coefficient on the numerical results was performed. To exclude numerical errors, a grid refinement analysis was carried out and is also presented in the paper.

Model description

A multidimensional two-fluid Eulerian approach is used for mathematical description of subcooled boiling flow. The governing equations of the two-fluid model have been extensively described in many works (e.g. [6]), thus they will not be repeated here. The numerical method of the CFX-5 code is based on finite volume discretization on collocated grid arrangement [7]. The liquid phase is dominant and is described as continuous while the vapour bubbles are described as a dispersed phase.

Turbulence modelling

Due to the lower density of vapour, it is commonly assumed that, in nucleate boiling flow, the motion of the dispersed vapour phase follows the fluctuations in the continuous liquid phase. Accordingly, the turbulence stresses are modelled only for the liquid phase, whereas the turbulence of the gaseous phase is not taken into account. The liquid phase turbulence is calculated by the two-equation k–ε model, which belongs to the category of eddy viscosity turbulence models. In bubbly two-phase flows, an additional production of liquid turbulence generated by fluctuating wakes behind the large bubbles may occur. The so-called bubble-induced turbulence is taken into account by additional viscosity term, which is added to the molecular viscosity of the liquid phase μ_l in the same way as the shear induced turbulence viscosity term μ_l^{turb}:

$$\mu_l^{eff} = \mu_l + \mu_l^{turb} + \mu_l^b . \tag{1}$$

Here μ_l^b represents the bubble-induced turbulence viscosity, which depends on the vapour phase volume fraction α, the local bubble diameter d_b and the relative velocity between the gaseous and liquid phase:

$$\mu_l^b = C_{\mu b}\rho_l \alpha d_b \left|\vec{u}_g - \vec{u}_l\right| . \tag{2}$$

Parameter $C_{\mu b}$ commonly takes the value 0.6, as recommended by Sato et al. [8]. Besides the turbulence intensity, the bubble diameter d_b also determines the interfacial momentum transfer (drag force, non-drag forces) and interfacial heat and mass transfer (condensation). Though the bubble size is a very important modeling parameter, in the present work a constant value of bubble diameter has been used, since bubble size was not measured in the considered ASU experiments.

Interfacial transfer

The interfacial transfer of momentum is modeled with the interfacial forces, which include drag force $\vec{F}_D$, lift force $\vec{F}_L$, turbulent dispersion force $\vec{F}_{TD}$ and wall lubrication force $\vec{F}_w$. The interfacial drag force is calculated as

$$\vec{F}_D = \frac{3}{4}\frac{C_D}{d_b}\alpha_g \rho_l \left|\vec{u}_g - \vec{u}_l\right|(\vec{u}_g - \vec{u}_l), \tag{3}$$

where C_D is the drag coefficient for bubble, which is flow-regime dependent and can be obtained experimentally. In the present study two different correlations for the drag coefficient have been used: the Schiller-Naumann [9] and Ishiii and Zuber [10] correlation. The later one is applicable for distorted bubbles. To predict a non-homogeneous radial void fraction distribution, the non-drag forces, which act perpendicularly to the flow direction, also need to be modeled. The lift force on the liquid phase can be calculated as

$$\vec{F}_L = \alpha C_L \rho_l \left(\vec{u}_g - \vec{u}_l\right) \times \nabla \times \left(\vec{u}_l\right), \tag{4}$$

where C_L is the lift force coefficient given by Tomiyama [11]. Lift force is shear-induced and pushes small bubbles towards the lower velocity region. The effect of dispersion of the vapor bubbles due the turbulent eddies in the liquid phase is taken into account by the turbulent dispersion force. In CFX-5 the turbulent dispersion force is based on the Favre averaging of the interfacial drag force [12]:

$$\vec{F}_{TD} = -\frac{3C_D \mu_l}{4 d_b \sigma_t}\left(\vec{u}_g - \vec{u}_l\right)\frac{\nabla \alpha}{1-\alpha}, \tag{5}$$

where μ_l is total dynamic viscosity of liquid and σ_t is the turbulent Schmidt number for the liquid phase. The contribution of the wall lubrication force in the subcooled boiling flow is probably the most difficult to evaluate, as it acts only on those near-wall bubbles which have already lift-off the wall. In the case, when there is some liquid flow between the bubble and the wall, the wall lubrication force acts in lateral direction away from the wall and prevents the accumulation of bubbles on the wall. Therefore the use of this force for wall boiling conditions is a subject of further investigation. Herein the model of Antal et al. [13] has been used for wall lubrication force:

$$\vec{F}_W = -\frac{\alpha \rho_l \left(\vec{u}_g - \vec{u}_l\right)^2}{d_b} \cdot \vec{n} \cdot \max\left(C_1 + C_2 \frac{d_b}{y_w}, 0\right), \tag{6}$$

where C_1 and C_2 are –0.05 and 0.01, respectively. The wall lubrication force approaches infinity as the wall distance approaches zero ensuring zero void fraction on the wall.

After departure from the heated wall, a bubble is surrounded by the subcooled liquid. The vapour inside the bubble and the bubble interface are assumed to be at saturation temperature. The interfacial condensation rate Γ_{cond} across the phase boundary is defined as

$$\Gamma_{cond} = \frac{h_{if} A_i \left(T_{sat} - T_l\right)}{h_{fg}}, \tag{7}$$

where A_i is the interfacial area per unit volume and h_{il} is the interfacial heat transfer coefficient modeled by widely used Ranz-Marshall correlation [14].

Wall boiling model

During subcooled boiling flow, heat and mass exchange between the phases takes place on the heated wall and in the subcooled liquid flow. On the heated surface the vapour bubbles are generated and as they move through the subcooled liquid they condense and release the latent heat. The bubble condensation is briefly described in the following section. The evaporation mass flow on the wall $\dot{m}_w$ is applied to the near-wall cell and is modelled in a mechanistic way, taking into account the total mass of bubbles periodically departing from nucleation sites:

$$\dot{m}_w = \left(\frac{\pi \cdot d_{bw}^3}{6}\right)\rho_g f \cdot N_a, \tag{8}$$

where d_{bw} is the bubble departure diameter, f is the bubble departure frequency and N_a is the nucleation site density. The boundary conditions for the heat transfer at the wall require a model for wall heat flux partitioning, which splits the total heat flux into the heat flux transferred to the liquid phase and the heat flux used to generate vapor. In the CFX-5 code a modified model of Kurul and Podowski [15] is implemented which splits the total wall heat flux into three different modes of heat transfer:

$$q_w = q_{1\Phi} + q_Q + q_e, \tag{9}$$

where $q_{1\phi}$ is the single-phase convection heat flux transferred to the liquid phase near the wall outside the area influenced by nucleating bubbles A_{bub}, q_Q is quenching heat flux transferred to the subcooled liquid from the bulk flow that fills the volume vacated by departing bubbles and q_e is the fraction of

the wall heat flux, that is directly used to generate vapor bubbles. The heat flux components are modeled as functions of local flow parameters, such as wall temperature T_w, liquid temperature T_l, latent heat h_{lg}, to list just a few. The single-phase convection heat flux is calculated using the single-phase blended linear-logarithmic temperature wall function of Kader [16]:

$$q_{1\phi} = \frac{\rho_l c_p u_w}{T^+_{y^+(nw)}} \cdot (1 - A_{bub}) \cdot (T_w - T_{l,(nw)}), \tag{10}$$

where $T_{l,(nw)}$ is the liquid temperature of the near-wall computational cell, $T^+_{y^+(nw)}$ is analytically calculated non-dimensional temperature [16] at the non-dimensional distance from the near-wall cell $y^+(nw)$ and u_w is the friction velocity. The single-phase convection heat flux takes place outside the area of nucleating bubbles ($1-A_{bub}$). To obtain a grid independent solution the quenching heat flux is assumed to be proportional to the temperature difference at a given distance from the wall:

$$q_Q = h_Q A_{bub} \left(T_w - T_{l,y^+(const)}\right). \tag{11}$$

In Eq. (11), h_Q is the quenching heat transfer coefficient and $T_{l,y^+(const)}$ is the liquid temperature at a given non-dimensional distance from the wall $y^+(const)$, which can be predefined. Taking into account the self-similarity of non-dimensional temperature profiles at different y^+, the temperature difference in Eq. (11) can be calculated as:

$$(T_w - T_{l,y^+(const)}) = \frac{T^+_{y^+(const)}}{T^+_{y^+(nw)}} (T_w - T_{l,(nw)}). \tag{12}$$

The use of a temperature wall function with the boiling model is a novel approach implemented in CFX-5 [3] and will be discussed later. The evaporation heat flux can be derived from the evaporation mass flux

$$q_e = \dot{m}_w h_{lg}. \tag{13}$$

The bubble influence area per unit wall area A_{bub} is determined as

$$A_{bub} = \min\left[1, N_a K \left(\frac{\pi d_{bw}^2}{4}\right)\right]. \tag{14}$$

The parameter K determines the size of the bubble influence area around the nucleation site on the heated wall that is subject to the quenching heat transfer. Commonly, the constant value of K = 4 is used. Thus, at high density of nucleation sites N_a and large bubble size, the bubble influence area is formally limited by the total heating surface (A_{bub}= 1). The overlapping between the two neighboring sites with asynchronous nucleating bubbles is neglected. In the current work two models for the bubble departure diameter have been used and validated. The model of Tolubinski [17]

$$d_{bw} = \min\left(1.4[mm], 0.6[mm] \cdot \exp\left(-\frac{\Delta T_{sub}}{45[K]}\right)\right) \tag{15}$$

is derived from the high-pressure water boiling experimental data with the upper limit for the bubble departure diameter (d_{bw} =1.4 mm). The upper correlation includes three adjustable parameters and depends solely on local liquid subcooling, which makes this correlation case dependent. Therefore a mechanistic model of Unal [18] based on fundamental principles of bubble evaporation on the heated plate has been implemented as well. The bubble size at detachment is influenced by pressure, wall material, wall superheating, local subcooling and by local velocity. The original correlation has been later modified [19] to be valid up to saturation:

$$d_d = 2.42 * 10^{-5} * p^{0.709} \frac{A}{\sqrt{bk}} \tag{16}$$

with

$$A = \frac{\Delta T_{sat}}{2\rho_g h_{\mathrm{lg}}}\left(\frac{k_w \rho_w c_w}{\pi}\right)^{0.5}, \tag{17}$$

$$b = \begin{cases} \dfrac{\Delta T_{sub}}{2\left(1-\rho_g/\rho_l\right)} & St < 0.0065 \\ \dfrac{1}{2\left(1-\rho_g/\rho_l\right)}\dfrac{q_w}{0.0065\rho_l c_{pl} u_l} & St > 0.0065 \end{cases}, \tag{18}$$

$$St = \frac{q_w}{0.0065\rho_l c_{pl} u_l \Delta T_{sub}}, \tag{19}$$

$$k = \max\left(1, (u_l/0.61)^{0.47}\right). \tag{20}$$

The variables f, N_a and h_Q are also calculated from empirical or semi-empirical equations which are basically the same as in the work of Kurul and Podowski [15]. The remaining unknown in equations for heat flux components (10, 11, 13) is the wall temperature T_w that can be calculated from the wall heat flux balance (9) with an iterative procedure using a bisection algorithm.

Near-wall treatment

The vapour phase at the wall boiling model is generated in the first near-wall cell. In the wall boiling model by Kurul and Podowski [15] the local variables (liquid velocity u_l, liquid temperature T_l) that appear in boiling correlations were taken from the near-wall cell. However, most of the constitutive relations (e.g. quenching heat flux, bubble departure diameter) are derived for one-dimensional thermal-hydraulic codes in terms of mean temperature and mean velocity. When these correlations are applied straightforwardly, as CFD boundary conditions simply by replacing averaged values by local ones, this would inevitably lead to the grid dependent solution. This works only for very coarse grids, where the first grid cell covers the entire boundary layer thickness. To ensure grid invariant solution in the CFX-5 code a characteristic temperature $T_{l,y^+(const)}$ was used instead of local near-wall temperature and was calculated from the analytical profile of the single-phase temperature wall function [16] at the given non-dimensional distance from the wall y^+. In the present study a constant value of $y^+=250$ is used. The proposed approach is a possible way to accommodate the existing correlations for CFD calculation. However, the use of single-phase wall function is questionable since it is known that the velocity and temperature profiles in the bubbly boundary layer deviate from single-phase counterparts [20], [21]. The upgrade of the model with some mechanistic two-phase wall function is therefore necessary. The research on this subject is currently underway.

Results and discussion

The two-fluid model described in the previous section was used to simulate Arizona State University (ASU) experiments. The ASU experimental setup is described in detail in [1]. The working fluid in the experiments was refrigerant R-113. The measurement section (also shown in Figure 1a) consists of a vertical annular channel with a heated inner tube (i.d.=14.6 mm, o.d.= 15.8 mm) and insulated outer tube (i.d.=38.02 mm, o.d.= 42.02 mm). The inner tube is made of stainless steel and the outer tube is made of plexiglass, except for the 0.521 m long measurement section which is made of optical quality quartz. The total length of the annular channel is 3.66 m and the 2.75 m long upper part of the inner tube is heated by the direct current. The 0.91 m long lower part of the annulus is not heated. The local measurements of transversal profiles of void fraction, phase velocities, velocity fluctuations and liquid temperature were performed at a single axial location located 1.99 m

downstream from the beginning of the heated section. For one experiment (*tp6* in Table 1) the local bubble diameter size was also measured, but the authors [1] did not carry out bubble size measurements for other experimental cases since they have concluded that these measurements are not accurate enough. The measurement probes and measurement techniques used in ASU experiments are described in the original paper of Roy et al. [1].

Table 1 Experimental conditions [1]

Exp. No.	$p_{m.p.}$ (bar)	q_w(kW/m^2)	G (kg/m^{2}s)	T_{sat} (^{o}C)	T_{inlet} (^{o}C)
tp1	2.69	95	568	80.5	42.7
tp2	2.69	116	568	80.5	42.7
tp3	2.69	95	784	80.5	42.7
tp4	2.69	116	784	80.5	42.7
tp5	2.69	95	784	80.5	50.2
tp6	2.69	116	784	80.5	50.2

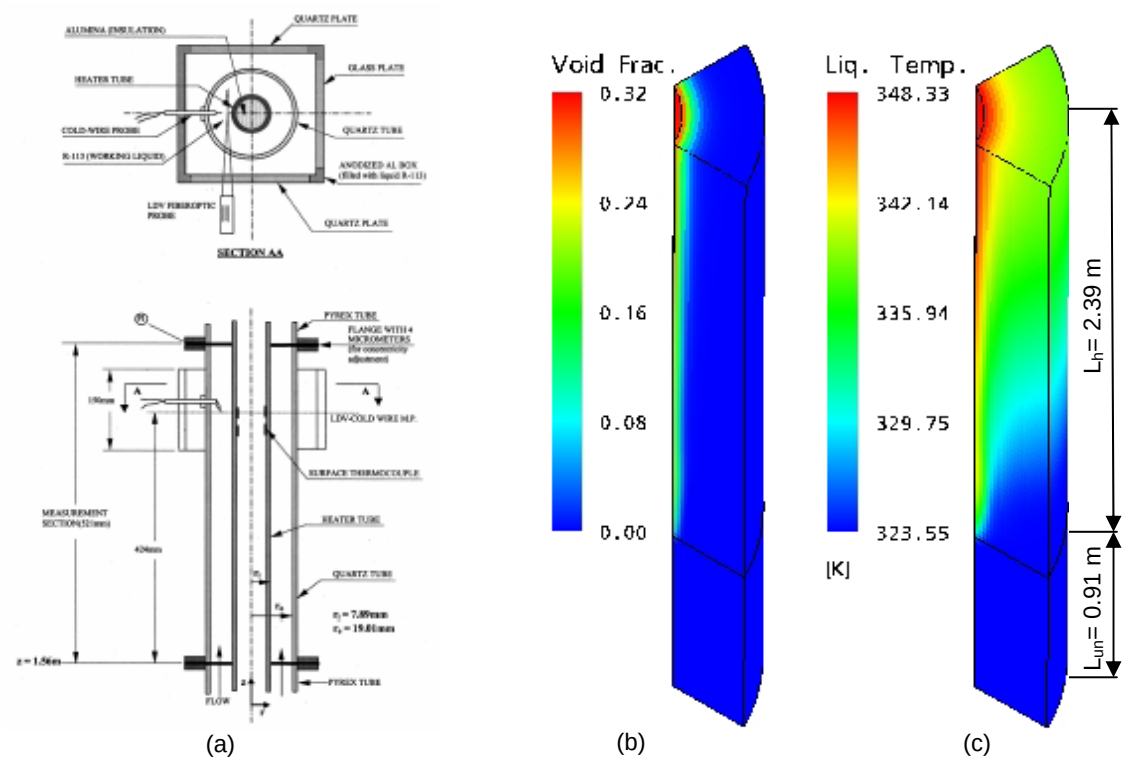

Figure 1 (a) The measurement section of ASU experiment (taken from [1]); (b) Calculated distribution of void fraction; (c) Calculated distribution of liquid temperature

Six experimental cases presented in Table 1 were simulated. The length of the simulated geometry was 3.3 m with 2.39 long upper heated part (Figure 1c). For the reference calculation the experimental case *tp6* was selected, since here also the local bubble size was measured. Figures 1 (b) and (c) show the distributions of the gas volume fraction and the liquid temperature in the annular channel. It should be noted that the presentation is deformed (it is much shorter) along the height. For the liquid phase a no-slip and for the gaseous phase a free slip boundary condition was used at the walls. A constant heat flux boundary condition was applied at the upper part of the inner wall. At the inlet, uniform velocity and temperature profiles were set according to Table 1. A pressure boundary

condition was applied at the annulus outlet. The CFX-5 calculations were run in the "steady-state" mode.

To obtain a geometry and grid invariant solution a grid refinement analysis for four 2D grids and one 3D grid was performed. The 3D geometry is modelled as a 60° sector of the annular channel with 19 grid cells in radial and circumferential directions and 110 grid cells along the channel height. The calculations on different grids (Figures 2(a) and (b)) show that the 2D grid with 19 cells in radial and 110 cells in axial direction is a good compromise between the numerical accuracy and the computational effort. Thus, all further calculations are performed on this grid. The solution was considered to converge if the mass flux G (kg/sm^2) was conserved along the channel height, which has been validated with the relative mass flux error:

$$err_G[\%] = \left(\frac{\left\langle \rho_l u_l \alpha_l + \rho_g u_g \alpha_g \right\rangle - G_{in}}{G_{in}} \right) \cdot 100, \tag{21}$$

where the first term in the numerator denotes the calculated mass flux averaged over the flow cross-section and G_{in} denotes the inlet mass flux. As shown in Figure 2 (c), the mass conservation (3D case) is very good, since the relative mass error remains below 0.02 % over the entire channel height.

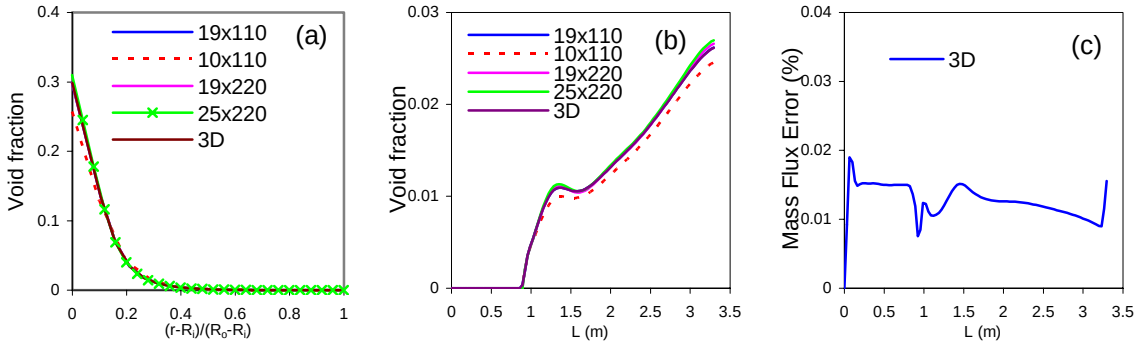

Figure 2 Grid and geometry influence on radial void fraction profile (a) and axial cross-section averaged void fraction (b); Relative mass flux error along the annulus height (c)

Comparison of experimental and simulation results

In Figures 3 to 7 the results of the "base" CFX-5 calculations are compared against the measured data of six experimental cases in Table 1. The radial profiles of different variables are measured and calculated at the axial location 2.9 m from the channel inlet. The following closure models and model parameters were used for the base CFX-5 calculation: the k–ε turbulence model for the liquid phase, the Sato model for the bubble induced turbulence, the Schiller-Naumann model of the interfacial drag, the Favre-averaged turbulence dispersion force (Eq. 5), the default Tolubinski model for the bubble departure diameter (Eq. 15) and the constant bulk bubble diameter size of 1.2 mm.

Figure 3 shows the measured and calculated radial void fraction radial profiles. The calculated void fraction shows a good agreement for the cases *tp3* and *tp4*, whereas some underprediction just near the wall may be observed for the remaining four cases. The discrepancy is somewhat higher for the cases *tp1* and *tp2*, which have a lower mass flux. The disagreement with the measured void fraction at changed mass flux conditions may be attributed mainly to the wall heat partitioning model.

The liquid velocities are compared in Figure 4. A common characteristic for all six cases is that the calculated liquid velocity in the high void fraction region near the heated inner wall is much higher than the measured one. As shown in Figure 5, the same holds also for the gas phase velocity. The overprediction of phase velocities by the multi-fluid CFD solvers in the two-phase flow region near the heated wall has been reported in many papers (e.g. [1], [19]). The calculation of the axial gas velocity depends on the model for interfacial drag and interfacial area density (e.g. bubble size)

whereas the axial liquid velocity profile in the wall boundary layer mainly depends on the wall friction, determined by the velocity wall function. Other influencing parameters are non-drag forces.

The turbulent kinetic energy profile calculated by the k–ε model shows qualitatively good agreement with the experimental data for all six cases (Figure 6). The liquid temperature profiles are compared in Figure 7. A very good agreement may be observed for all cases, except for the case *tp2*, where calculated temperature values are somewhat higher than experimental ones.

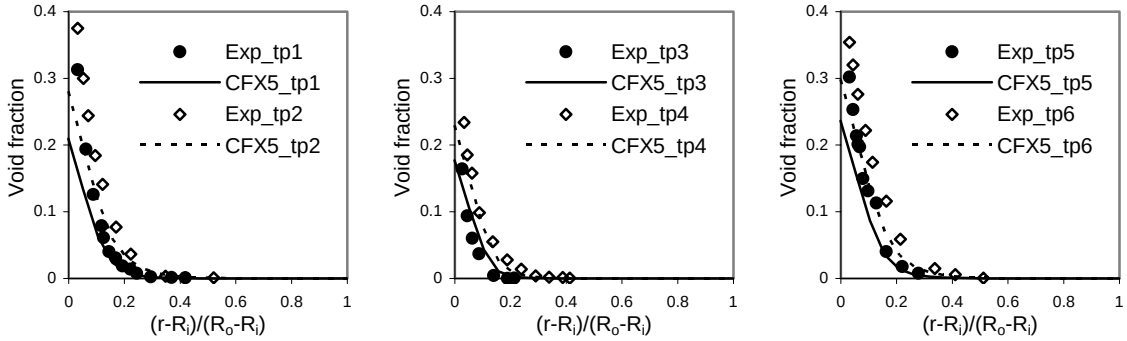

Figure 3 Calculated vs. experimental void fraction profile

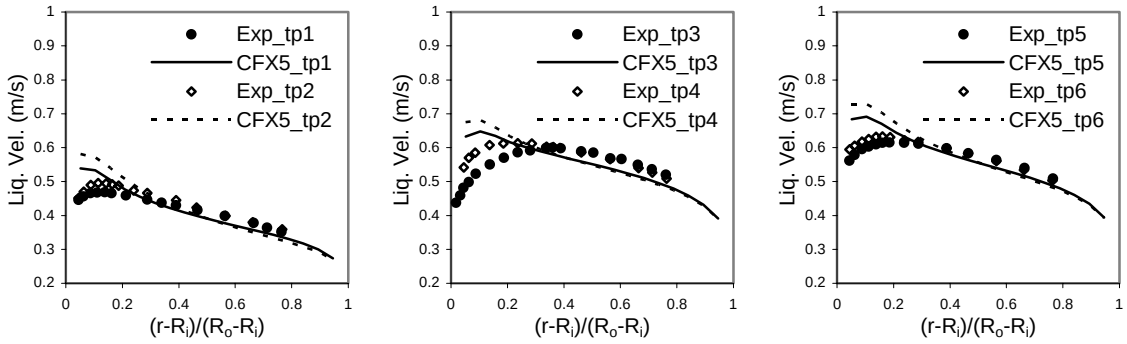

Figure 4 Calculated vs. experimental liquid velocity profile

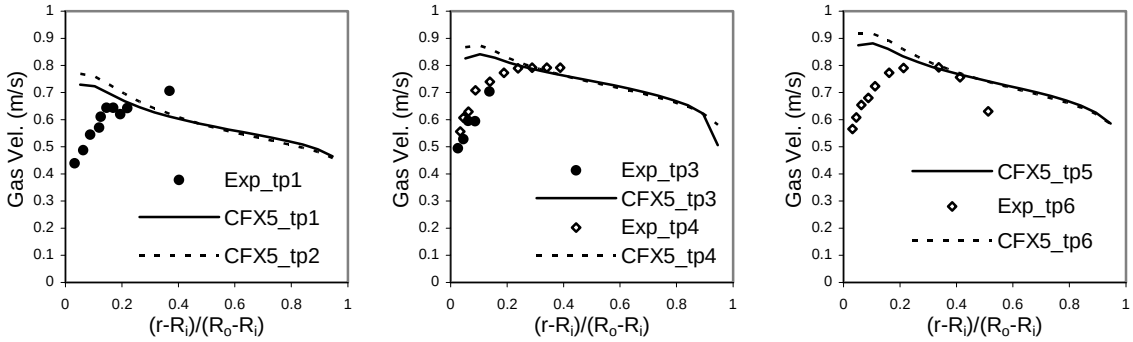

Figure 5 Calculated vs. experimental gas velocity profile

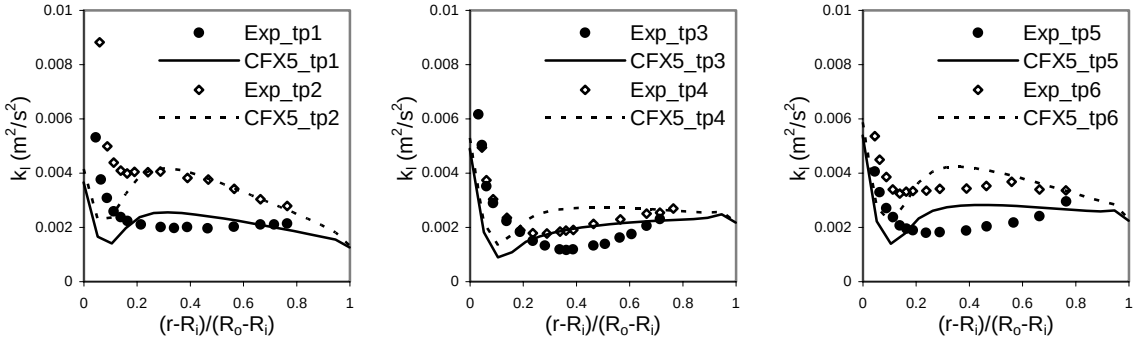

Figure 6 Calculated vs. experimental turbulent kinetic energy profile

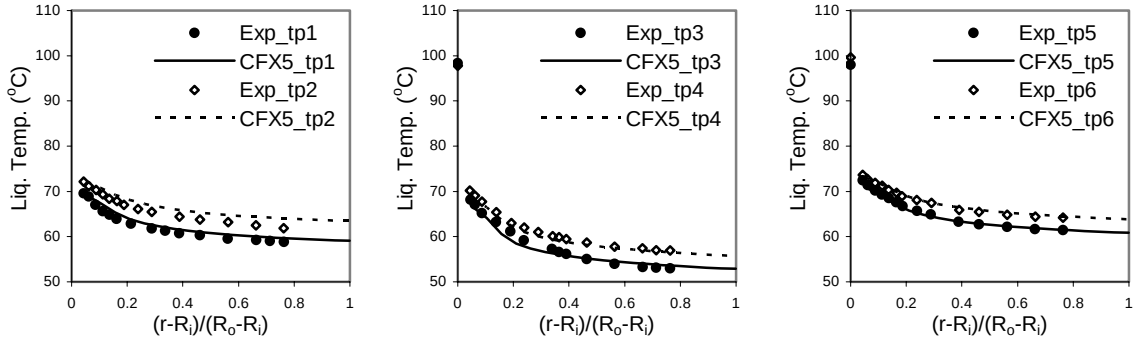

Figure 7 Calculated vs. experimental liquid temperature profile

Sensitivity analyses

To investigate possible causes for discrepancies between the calculations and the measured data in the previous section, the sensitivity analysis of some model parameters were performed on the reference case *tp6*. These include the effect of non-drag forces, bubble diameter size and the effect of different models for interfacial drag coefficient.

Non-drag forces

Separate effects of non-drag forces in boiling (turbulent dispersion force, lift force, wall lubrication force) were investigated in Figure 8. The lift force is proportional to the liquid velocity gradient therefore the inclusion of the lift force slightly increases the void fraction near the wall and slightly decreases the void fraction away from the wall. The wall lubrication force has the strongest influence on the void fraction and somewhat smaller also to the liquid velocity profile.

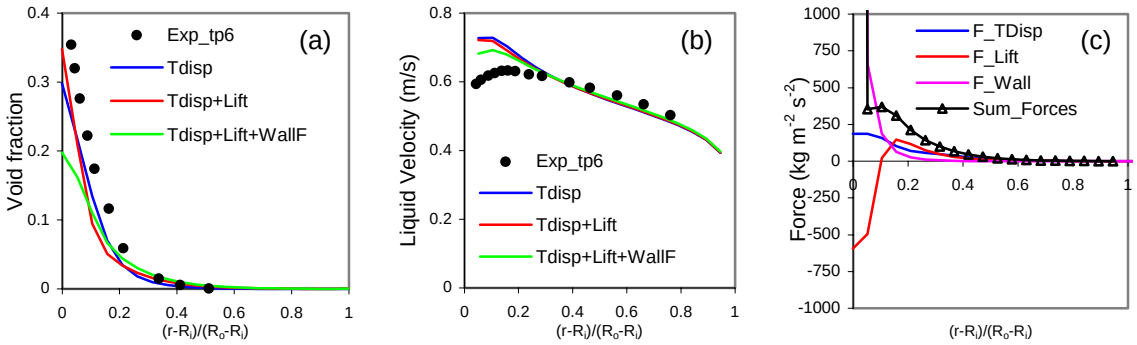

Figure 8 Influence of Non-drag forces; (a) void fraction profile; (b) liquid velocity profile; (c) non-drag force values

Although the implementation of the wall lubrication force is necessary for the adiabatic two-phase flows, as it reproduces the void fraction peak near the wall [23], it leads to underprediction of the near-wall void fraction for the presented wall boiling case. The use of wall lubrication force might be questionable for the spherical-cap bubbles continuously growing and/or sliding on the heated wall. According to its formulation a zero void fraction at the wall is required. The well known Antal formulation of the wall force (Eq. 6) with reciprocal linear relation to the wall distance (1/y) formally contradicts with the non-zero wall source of dispersed phase, since its integral across the boundary layer is infinitely large. However, the use of wall lubrication force was proved to be advantageous for the conditions of low-pressure boiling of water [24]. Further research is necessary to improve the existing wall force models.

Bubble size

The bubble size varies along the flow, as well as in the normal direction to the flow. Vapour bubbles generated at the heated wall may slide along the wall, eventually depart and travel further with the subcooled flow, where they are subjected to heat and mass exchange and to the turbulent liquid velocity field. Bubble size is a very important modelling parameter. Local bubble diameter size defines the interfacial area density in the bulk flow, which influences the interfacial momentum transfer terms (drag force, wall lubrication force) and interfacial heat and mass transfer terms (bulk condensation and evaporation). The bubble departure diameter is included in the wall boiling model and directly affects the amount of gas phase generated on the heated wall. For the preliminary simulations in this paper each diameter (in the bulk and at departure) is modelled separately. As reported in [1] the measured most probable bubble diameter size for the case *t6* was between 0.7 mm and 1.2 mm. Since the bubble diameter was measured at only one axial location a constant bubble diameter over the entire computational domain was adopted in simulations. In Figure 9 the influence of bubble diameter size on the results is presented. The case "db=1.2mm" denotes the base calculation with bulk diameter of 1.2 mm and Tolubinski model for the bubble departure diameter. As shown in Figure 9 (a), the smaller bulk bubble diameter (0.7 mm) increases the condensation rate, the two-phase region is narrower and more gas phase is accumulated near the wall. The smaller bubble diameter also decreases relative velocity between the phases, but it does not influence the liquid axial velocity profile (Figure 9 (a)). The influence on the liquid temperature is negligible (Figure 9 (c)). The changed correlation for bubble departure diameter (Unal model in Eq. 16) results in somewhat lower values of void fraction near the wall, whereas the influence on phase velocities and liquid temperature is negligible.

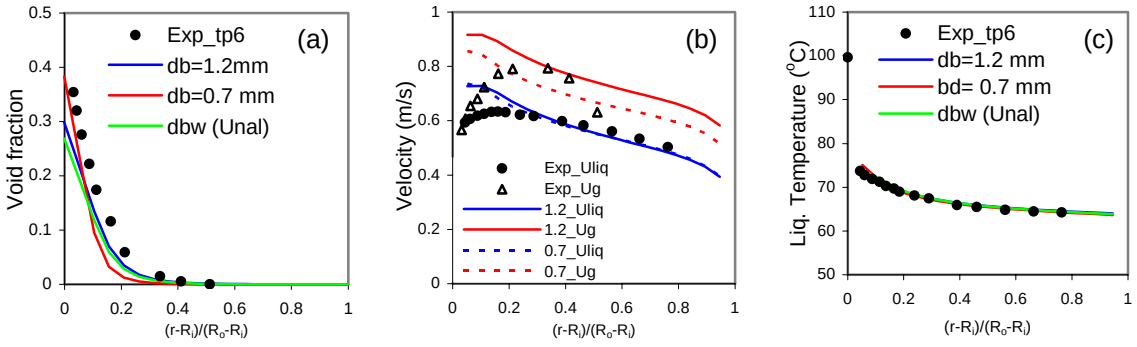

Figure 9 Influence of bubble diameter: radial void fraction profile (a); radial liquid and gas velocity profiles (b); radial liquid temperature profile (c)

Interfacial drag coefficient

The influence of different interfacial drag coefficients is presented in Figure 10. The Ishii-Zuber drag coefficient results in a higher interfacial drag and consequently lower gas velocity. As expected the liquid velocity is not affected, but the void fraction values near the wall are higher and closer to the measured values. The influence on the liquid temperature is negligible (Figure 10 (c)).

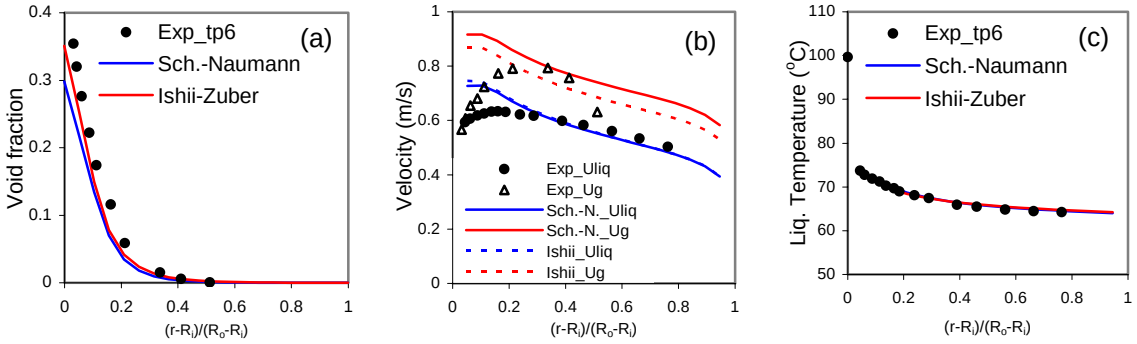

Figure 10 Influence of interfacial drag: radial void fraction profile (a); radial liquid and gas velocity profiles (b); radial liquid temperature profile (c)

Conclusions

A forced convective boiling of Refrigerant R-113 in a vertical annular channel has been simulated by a state-of-the-art two-fluid model of the CFX-5 code. Grid independent solution on dense grids was obtained by using adequate near-wall treatment, based on the analytical temperature wall function. The simulation results have been validated against the Arizona State University (ASU) experimental data [1]. Earlier [4], the same two-fluid model has been successfully validated against the water-steam experiments in vertical pipes at high pressure conditions (30–150 bar). In the present work, a qualitatively good agreement with the ASU experiments in the annular channel has been achieved without changing model parameters. This shows that the current two-fluid model may be successfully applied also for other working fluids and different channel geometries. The influence of non-drag forces, bubble diameter size and interfacial drag model on the numerical results has been investigated as well. However, a lot of research problems still remains to be resolved to correctly predict the evolution of boiling flow structure along the channel. The ongoing research is focused on the development of the two-phase wall function aiming to improve the prediction of liquid velocity profile. In the near future the improvement of interfacial force models, local bubble size modelling and the improvement of the heat flux partitioning model should be tackled.

Acknowledgement

The financial support from the Slovenian Research Agency for the project "Three-dimensional Eulerian model of convective boiling" (Z2-6651) is gratefully acknowledged.

References

[1] R.P. Roy, S. Kang, J.A. Zarate, A.Laporta, "Turbulent subcooled boiling flow – experiments and simulations", *J. Heat Transfer* **124**, 2002, pp. 73-93.

[2] J.M. Delhaye, F. Maugin, J.M. Ochterbeck, Void fraction predictions in forced convective subcooled boiling of water between 10 and 18 MPa, *Int. J. Heat Mass Transfer* **47**, 2004, pp. 4415-4425.

[3] Y. Egorov, F. Menter, Experimental implementation of the RPI wall boiling model in CFX-5.6, Technical Report ANSYS/TR-04-10, ANSYS GmbH, 2004.

[4] B. Koncar, E. Krepper, Y. Egorov, CFD Modelling of Subcooled Flow Boiling for Nuclear Engineering Applications, International Conference, Proc. *Nuclear Energy for New Europe*, Bled, Slovenia, September 5-8, 2005.
[5] E. Krepper, Y. Egorov, CFD-modelling of subcooled boiling and application to simulate a hot channel of a fuel assembly, *Proc. 13th Int. Conf. Nuclear Engineering (ICONE-13)*, Beijing, China, May 16-20, 2005.
[6] M. Ishii, Thermo-fluid dynamic theory of two-phase flow, Eyrolles, Paris, 1975.
[7] CFX-5 Documentation, Solver Theory, Multiphase Flow Theory, ANSYS, 2004.
[8] Y. Sato, M. Sadatomi, K. Sekoguchi, Momentum and heat transfer in two-phase bubble flow - I. Theory, Int. J. Multiphase Flow 7 (1981) 167-177.
[9] L. Schiller, A. Naumann, *VDI Zeits* **77**, 1933, pp. 318.
[10] M.Ishii, N.Zuber, Drag coefficient and relative velocity in bubbly, droplet or particulate flows, AIChE J. 25 (1979) 843-855.
[11] A. Tomiyama, Struggle with computational bubble dynamics, *Third Int. Conf. Multiphase Flow, ICMF-1998,* Lyon , France, June 8-12, 1998.
[12] A.D. Burns, T. Frank, I. Hamill, J.M. Shi, The Favre averaged model for turbulence dispersion in Eulerian multi-phase flows. *5th Int. Conf. Multiphase Flow, ICMF-2004,* Yokohama, Japan, 2004.
[13] S.P. Antal, R.T. Lahey Jr., J.E. Flaherty, Analysis of phase distribution in fully developed laminar bubbly two-phase flow, Int. J. Multiphase Flow 17 (1991) 635-652.
[14] W.E. Ranz,, W.R. Marshall, Evaporation from drops, *Chemical engineering progress* **48**, No. 3, 1952, pp. 141-146.
[15] N. Kurul, M.Z. Podowski, Multidimensional effects in forced convection subcooled boiling, in: Proceedings of the Ninth International Heat Transfer Conference, August 19-24, Jerusalem, Israel, Vol. 2, pp. 21-26, 1990.
[16] B.A. Kader, "Temperature and concentration profiles in fully turbulent boundary layers", *Int. J. Heat Mass Transfer* **24**, 1981, pp. 1541-1544.
[17] V.I. Tolubinski, D.M. Kostanchuk, Vapour bubbles growth rate and heat transferintensity at subcooled water boiling, 4th Int. *Heat Transfer Conf., Vol. 5, paper No. B-2.8,* Paris, 1970.
[18] H.C. Unal, Maximum bubble diameter, maximum bubble-growth time and bubble-growth rate, *Int. J. Heat Mass Transfer* **19,** 1976, pp. 643-649.
[19] C. Morel, S. Mimouni, J.M. Laviéville, M. Boucker, R113 boiling bubbly flow in an annular geometry simulated with the NEPTUNE code, *Proc. NURETH-11,* Avignon, France, 2005.
[20] A.A. Troshko, Y.A. Hassan, "A two-equation turbulence model of turbulent bubbly flows", *Int. J. Multiphase Flow* **27**, 2001, pp. 1965-2000.
[21] B. Končar, E. Krepper, Y.A. Hassan, Two-Phase Boundary Layer Prediction In Upward Boiling Flow, *Proc. Int. Conf. Nuclear Energy for New Europe 2004*, Portorož, Slovenia, Sept. 6-9, 2004.
[22] W. Yao, C. Morel, "Volumetric interfacial area prediction in upward bubbly two-phase flow", *Int. J. Heat Mass Transfer* **47**, 2004, pp. 307-328.
[23] D. Lucas, E. Krepper, H.-M Prasser, Development of co-current air-water flow in a vertical pipe, *Int. J. Multiphase Flow* **31**, 2005, pp. 1304–1328.
[24] B. Končar, I. Kljenak, B. Mavko, Modelling of local two-phase flow parameters in upward subcooled flow boiling at low pressure. *Int. J. Heat Mass Transfer* **47**, 2004, pp. 1499-1513.